HOKKAIDO UNIVERSITY

Title	Structural and electromagnetic characterizations of Fe-SrF2 granular films
Author(s)	Hosoya, H.; Arita, M.; Hamada, K. et al.
Citation	Journal of Physics D: Applied Physics, 39(24), 5103-5108 https://doi.org/10.1088/0022-3727/39/24/001
Issue Date	2006-12-21
Doc URL	https://hdl.handle.net/2115/29630
Rights	Copyright © 2006 IOP Publishing Ltd.
Type	journal article
File Information	JPD39-24.pdf

Hokkaido University Collection of Scholarly and Academic Papers : HUSCAP

Structural and electromagnetic characterizations of Fe-SrF_2 granular films

H. Hosoya[1], M. Arita[1], K.Hamada[1], Y. Takahashi[1], K. Higashi[2], K. Oda[2], and M. Ueda[3]

[1] Graduate School of Information Science and Technology, Hokkaido University, Sapporo 060-0814, Japan

[2] Institute of Industrial Science, University of Tokyo, Meguro-ku, Tokyo 153-8505, Japan

[3] Graduate School of Engineering, Hokkaido University, Sapporo 060-0813, Japan

E-mail: hosoya@nano.ist.hokudai.ac.jp

Abstract.

We investigate composite Fe-SrF_2 films to explore new materials showing the granular type tunneling magnetoresistance (TMR) effect. The films are composed of Fe nano-particles embedded in a SrF_2 matrix. The electromagnetic properties of the ferromagnetic metal-insulator films are confirmed, including super-paramagnetism, tunnel conduction, and TMR. We obtain a TMR of 3% at RT and 5% at 77 K. The film resistivity is much higher than that of oxide-based granular film. We also fabricate the nanostructures of granular films and aim at the application of the single-electron transistor. As a result, we observed Coulomb blockade (CB) region and CB oscillation at low temperature.

Keyword

Fe, SrF_2, granular thin films, magnetoresistance

PACS number: 73.40.Gk, 75.75.+a, 73.23.Hk, 81.05.Rm

1. Introduction

Spin-dependent electron tunneling giving the tunneling magnetoresistance (TMR) effect is intensively studied [1]. The tunnel current path is switched on and off by changing the magnetization directions of ferromagnetic (FM) layers composing the devices. Recently magnetic nanostructures have been fabricated, and single-electron tunneling (SET) effect has occurred in small particles. The interplay of spin dependent tunneling and SET effect in small magnetic metal particles has attracted much attention [2-6].

Metal-insulator granular films composed of metallic nanodots embedded in the insulating matrix have been frequently investigated to study the tunneling conduction of nanodot systems [7]. In ferromagnetic metal (FM)-insulator granular films, networks of magnetic tunnel junctions are formed. Thus, the TMR effect due to spin-dependent tunneling between neighboring FM dots has been intensively studied [8–15]. It is easy to produce such small metallic particles at granular systems. The granular films are useful for the study of the interplay of spin dependent tunneling and SET effects. Using a patterned FM-insulator granular film, Mitani et al. [16] have fabricated two-terminal devices and reported an enhancement in the TMR effect at a conventional low temperature by higher-order tunneling in Coulomb blockade regime. To further develop functional ferromagnetic SET devices (SEDs) such as a three-terminal ferromagnetic single-electron transistor, exploration of insulating materials used

in granular films is thought to be helpful. However, the materials reported so far are mainly oxides [8–12, 16]. Fluorides having high resistivity due to the wider band gap and smaller dielectric constants than MgO and Al_2O_3 are other possible candidates [20], but reports on FM-fluoride granular films have been rare [13–15].

In this work, we studied Fe-SrF_2 granular films. The insulating material SrF_2 was often used as optical material [17], and the epitaxial growth on Si substrate was studied [18, 19]. However, the Fe-SrF_2 granular system has not yet been reported on. Therefore, to learn the general features of this composite system, basic experiments to investigate the microstructure, the chemical state of Fe, magnetization, and the TMR properties were carried out. At the end of this article, we also briefly present how the granular films were nanofabricated and what the electric properties of a single-electron transistor composed of this granular film.

2. Experimental Procedure

2-1. Fe-SrF_2 granular films

Granular films were prepared by co-evaporating Fe and SrF_2 using a home-made ultra-high vacuum evaporator (base pressure: $<10^{-7}$ Pa) attached by two electron beam guns, with which eight samples having different compositions can be simultaneously prepared. The deposition was performed on MgO (001) surfaces kept at Ts = 300 K under a vacuum better than 6×10^{-6}

Pa. The deposition rate of SrF_2 was kept constant (typically 0.1 nm/s) and that of Fe was changed between 0.05 and 0.15 nm/s depending on the composition. The film thickness was between 150 and 250 nm depending on the composition. No cap layers were formed on the film surface. The composition was estimated by means of electron probe micro analysis (EPMA) by assuming that the Fe and SrF_2 densities are those of the bulk materials.

The film structure was observed by atomic force microscopy (AFM) in air, scanning tunneling microscopy (STM) in a vacuum, and transmission electron microscopy (TEM). The chemical states of Fe, Sr, and F were investigated by X-ray photoelectron spectroscopy (XPS, monochromated AlKα). The magnetization curves (MH curves) were measured at RT using a vibrating sample magnetometer (VSM). Electrical resistance measurements at RT and 77 K were performed mainly by the DC four-terminal method under the constant current mode. Occasionally, for the samples with high resistance values, two-terminal measurements under the constant voltage mode were carried out. In the magnetoresistance (MR) measurements, the magnetic field was applied along the sense current. The MR ratio was defined as MR(%) = 100 × $(\rho_{max} - \rho_{4kOe}) / \rho_{max}$, where ρ_{max} and ρ_{4kOe} are the maximum resistivity and resistivity under the magnetic field of 4 kOe (3.2×10^5 A/m).

2-2. Patterned Fe-SrF_2 devices

The single-electron transistors were fabricated on thermally oxidized silicon (001) substrates.

The thickness of the oxide layer was 200 nm. The patterns were formed using electron beam lithography and a lift-off process. First, the source and the drain electrodes made of Au (50 nm) / Cr (10 nm) were prepared. The gap length between these electrodes was approximately 50 nm. Afterwards, the Fe-SrF_2 granular films (20-nm thick) were deposited in a molecular beam epitaxy apparatus (base: ~10^{-8} Pa). During deposition, the samples were rotated to keep homogeneity. Finally SrF_2 (50 nm) was deposited to prevent oxidization. The pattern size of the deposited granular film was typically 2500 nm in length and 400 nm in width. The obtained devices were measured at 8 K in a cryogenic probing system (Nagase, GRAIL-20-305-6-LV) using a semiconductor parameter analyzer (Agillent, 4156C). For the measurements, the substrate Si was used as a gate terminal.

3. Results and discussion

3-1. Microstructure of Fe-SrF_2 granular films

In Figs. 1(a)–(c), AFM images of three samples are presented. In Fig. 1(a) for 26 vol.% Fe, the surface was composed of asperities with an in-plane size of several tens of nanometers. Some asperities are much more than 10 nm in height. The Ra value used to estimate surface roughness was 1.8 nm. The film of 52 vol.% Fe had a smooth surface with Ra = 0.9 nm (Fig. 1(b)). By an increment of an Fe fraction (Fig. 1(c)), the surface was rougher (Ra = 1.2 nm) than that of Fig.

1(b). For 20 samples with different Fe fractions, the in-plane sizes were between 40 and 60 nm without any systematic change depending on the Fe fraction. The Ra values are summarized in Fig. 1(d), where the surface roughness shows the minimum value at approximately 50 vol.% Fe. Although the reason for this is obscure, the roughness must contain some information about the crystal growth of this granular system. To study the geometry of Fe nano-particles in detail, STM observation was also carried out. In Fig. 1(e), an example is shown (ca. 30 vol.% Fe). Particles with a size of some nanometers can be seen. They are thought to be Fe particles, since Fe particles constitute the conduction path during the STM observations. Correspondingly, a TEM image indicates the existence of nano-particles (dark round contrast) in Fig. 1(f). There are many particles with diameters ranging from 2 to 5 nm in diameter and a bright network-like pattern covering the entire area. This is the SrF_2 matrix forming the tunnel barrier among the Fe particles.

Figure 2 contains an XPS spectrum showing the chemical states of (a) Fe, (b) Sr, and (c) F. To remove surface contamination and oxidized layers at the surface, the film was gently sputter-etched (Ar^+, 2 kV, 10 min). The two peaks in Fig. 2(a) are from metallic Fe, and the signal from FeF_2 (arrow, 711.4 eV) is weaker than the detection limit of the instrument. This was true also for another film investigated in this work. By assuming that the Fe particle size is 5 nm and the single atom layer at the particle surface is FeF_2, the intensity of the FeF_2 peak must be about 30% of that of metallic Fe. Therefore, we can conclude that no iron fluoride was

formed in this sample. The peaks in Figs. 2(b) and (c) correspond to those from SrF_2 (Sr: 133.5 and 135.2 eV, F: 684.8 eV) [21]. Composition estimation using these data gives a relationship of Sr : F = 1 : 1.9. Although fluorine can be slightly decomposed by electron beam evaporation, the strontium fluoride used is SrF_2. In conclusion, nanometer-sized Fe particles are dispersed in the SrF_2 matrix.

3-2. Magnetic and electronic properties of Fe-SrF_2 films

The typical results of electromagnetic measurements are presented in Fig. 3. In the resistivity vs. temperature (ρT) curve (Fig. 3(a)), the resistance is relatively high and a negative temperature coefficient was seen. At a low temperature depressing the thermal agitation, the CB effect was enhanced, and thus the resistivity was high. The electrical resistivity in metal-insulator granular systems has been theoretically investigated in terms of tunneling conductance between particles [7]. The dependence of resistivity (ρ) on temperature (T) is expressed by

$$\rho = \rho_0 \exp(T_0/T)^{1/2}, \qquad (1)$$

where ρ_0 and T_0 are constants. Considering above relation, a log ρ vs. $T^{-1/2}$ curve in Fig. 3(b) was almost linear with a slight curve. This indicates that the quality of dispersion is acceptable, while there must be some inhomogeneity in dispersion.

The MH curve is shown in Fig. 3(c). The magnetization is much smaller than the value of bulk Fe (220 emu/g_{Fe} = 2.17 Wb/m^2). Probably the magnetic correlation between the Fe atoms at the

particle surface was weak and the Fe-particles near the film surface were partly oxidized. The curve shows no hysteresis caused by the coercive force (H_c). Figure 3(d) is the resistivity dependence on the applied magnetic field, i.e., the MR curve. A clear negative MR effect was obtained. The three types of data discussed here are characteristic of FM metal-insulator granular films showing the TMR effect between metallic nano-particles.

Ferromagnetic nano-particles are known to have a super-paramagnetic feature, and the magnetization curve is expressed using the Langevin function (L),

$$M/M_S = L(\alpha) \equiv \coth\alpha - 1/\alpha , \qquad (2)$$

where M_S is the saturation magnetization. Parameter α is the ratio between the magnetostatic energy of one particle (μH where μ and H are the magnetic moment of a particle and the applied field, respectively) and its thermal energy (k_BT where k_B is the Boltzmann constant) and described by

$$\alpha = \frac{\mu H}{k_B T} = \frac{4\pi}{3}\left(\frac{d}{2}\right)^3 \frac{M_{Fe} H}{k_B T}, \qquad (3)$$

where M_{Fe} is the magnetization of Fe particles and d is the particle diameter. In granular films, a particle size distribution is expected. Generally, the log normal distribution function described below is used [22, 23].

$$f(d) = \frac{1}{\sqrt{2\pi}\ln\sigma}\exp\left[-\frac{(\ln d - \ln d_m)^2}{2\ln^2\sigma}\right], \qquad (4)$$

where d_m is the median and σ is the dispersion. Using Eq. (4), Eq. (2) becomes,

$$M = N\int M_{Fe}\frac{4\pi}{3}\left(\frac{d}{2}\right)^3 f(d)L(\alpha)\,\mathrm{d}d\,, \qquad (5)$$

where N is the number of particles.

Figure 4(a) shows the MH curve in Fig. 3(c) (35 vol.% Fe) superposed by the fitted curve based on Eq. (5). This fitting shows good agreement with the experimental data. The size distribution obtained in this process is shown in Fig. 4(b). The parameters σ and d_m were 1.73 and 1.62 nm. Thus, average particle size $d_{ave} \equiv \Sigma\{f(d)d\}/\Sigma f(d)$ was estimated to be 2.59 nm. This value corresponds to the results from the STM and TEM experiments.

The resistivity and MR ratios are summarized in Fig. 5 as a function of Fe fraction. The sample of 62 vol.% Fe showed a ρT curve with a positive temperature coefficient indicating metallic conduction. Correspondingly, anisotropic magneto-resistance (AMR) with a ratio of 0.01% was observed. By reducing Fe fraction, resistivity gradually increased and was two to three orders larger at about 40–50 vol.% Fe, which is the percolation fraction. Around this point in the graph, the MR ratio abruptly increased. At this fraction, the major conduction process changed to that of electron tunneling. The Fe fraction discussed here corresponds to the one giving the minimum surface roughness of the films. By further reducing the Fe fraction, the MR ratio decreased after the maximum value of 3.5% (RT, 35 vol.% Fe). This is due to the appearance of super-paramagnetism giving a broad MR curve. At 77 K, however, the thermal agitation was depressed, and the MR ratio continued to increase to the maximum value of 5% in this study. At

present, the MR ratio was smaller than other granular systems. It is thought that a part of Fe particles were oxidized because our granular films had not cap layers.

The electromagnetic results discussed here are qualitatively the same as those reported for many oxide systems reported previously [8–12]. One major difference is the value of resistivity. In Fig. 5(a), data for Fe-SrF_2 and Fe-MgO are compared; the data were prepared using the same method in our research group. The resistivity of the Fe-SrF_2 system is two to three orders larger than that of the Fe-MgO system. This tendency was recognized in the MgF_2 systems [15]. One possible explanation is the difference in the gap energies (e.g., 11.25 eV for SrF_2 and 7.3 eV for MgO [20]), while the difference in microstructure still remains as one cause of this phenomenon.

3-3. SET properties of Fe-SrF_2 devices

In the former section, we stated that the Fe-SrF_2 granular films have the fundamental properties of an FM-insulator. In this section, the SET characteristics of patterned Fe-SrF_2 devices are presented.

An SEM image of the device is shown in Fig. 6(a). The size of the granular film between the electrodes was about 50 nm long, 400 nm wide, and 20 nm thick, and the Fe fraction was 33 vol.%. By assuming a particle size of 3 nm and an SrF_2 barrier width of 1 nm, the number of Fe particles in this area is estimated to be approximately 9×10^3.

Fig. 6(b) shows the current-voltage (I_d-V_d) curves of the sample measured at 8 K (solid line) and at RT (dashed line). The gate voltage V_g was set at 0 V. Note that the vertical scales for 8 K and RT differ from each other by 1000 times. At RT, the data was almost linear, and the current flow was in the nA order. At 8 K, the drain current was suppressed down to the pA order, and the I_d-V_d curves showed strong nonlinearity similar to that of the SET junctions. The current did not flow around zero drain bias voltage as shown in Fig. 6(b). The CB effect was clearly achieved in this device. The threshold voltage estimated from an asymptotic line which lifted down from the value at 1 V was about 0.6 V.

In general, the appearance of SET is confirmed by the I_d response against the V_g modulation. Therefore, the I_d curves as a function of V_g were measured at 8 K for various drain voltages V_d around the CB regime (Fig. 6(c)). In each curve, a systematic I_d change can be seen. The curves were reproducibly observed. The period of the current oscillations was roughly estimated as ΔV_g = 35 V. These oscillation curves under different V_d showed the same peak positions as each other, while the peak-to-valley current ratio decreased with an increase of V_d. These are clear evidence of the CB oscillations.

4. Summary and Conclusion

Using the co-evaporation method, Fe-SrF_2 composite films were prepared on MgO (001). These are granular-type films where Fe nano-particles are embedded in an SrF_2 matrix. After electric

and magnetic measurements, the films were confirmed to show TMR and superparamagnetism. Tunneling magnetoresistance ratios of 3% (RT, 4 kOe) and 5% (77 K, 4 kOe) were observed. Although these values are not yet satisfactorily large, the principal properties of a FM-insulator granular film were recognized. The resistivity was two to three orders larger than that of oxide systems.

In nanofabricated Fe-SrF_2 granular films, the strongly nonlinear *I-V* characteristics and drain current oscillation as a function of gate voltage were observed. These are fundamental properties of a single-electron transistor. The next step of this research is to investigate the TMR measurements in detail around the Coulomb Blockade regime under various V_g values in order to be given a guideline to develop single-electron tunneling-TMR hybrid devices.

5. Acknowledgments

The EPMA analyses were performed with the help of Dr. Miyazaki. The STM observations were carried out by Dr. Hirose, Dr. Subagyo, and Prof. Sueoka. We also wish to acknowledge Professors Yamanoto and Shibayama for permission to use their AFM and TEM, respectively. A part of this work was supported by a Grant-in-Aid for the Japan Society for the Promotion of Science (Nos. 16206038, 17201029 and 18560640 and MOST through the Frontier 21 National Program for Tera-level Nano-Devices (TND) of Korea), for which we are most grateful. We are also grateful to the Suhara Memorial Foundation for financial support.

References

[1] Miyazaki T and Tezuka N 1995 *J. Magn. Magn. Mater.* **139** L231–4

[2] Ono K, Shimada H and Ootuka Y 1997 *J. Phys. Soc. Jpn.* **66** 1261–4

[3] Bruckl H, Reiss G, Vinzelbelg H, Bertram M, Monch I and Schumann J 1998 *Phys. Rev. B* **58** R8893-6

[4] Takahashi S and Maekawa S 1998 *Phys. Rev. Lett.* **80** 1758-61

[5] Iwabuchi S, Tanamoto T and Kitawaki R 1998 *Physica B* **249-251** 276-80

[6] Barnas J and Fert A 1998 *Phys. Rev. Lett.* **80** 1058-61

[7] Abeles B, Sheng P, Coutts M D and Arie Y 1975 *Adv. Phys.* **24** 401–61

[8] Fujimori H, Mitani S and Ohnuma S 1995 *Mater. Sci. Eng.* **B31** 219–23

[9] Milner A, Gerber A, Groisman B, Karporsky M and Gladkikh A 1996 *Phys. Rev. Lett.* **76** 475–8

[10] Hayakawa Y, Hasegawa N, Makino A, Mitani S and Fujimori H 1996 *J. Magn. Magn. Mat.* **154** 175–82

[11] Huang Y H, Hsu J H and Chen J W 1997 *IEEE Trans. Magn.* **33** 3556–8

[12] Boff M A S, Teixeira S R, Schmidt J E and Antunes A B 2004 *Appl. Phys. Lett.* **85** 757-8

[13] Furubayashi T and Nakatani I 1996 *J. Appl. Phys.* **79** 6258–60

[14] Ono K, Yasui C, Yanagihara H, Koyano T, Ota K and Kita E 2002 *Jpn. J. Appl. Phys.* **41** 97–102

[15] Kobayashi N, Ohnuma S, Masumoto T and Fujimori H 2000 *J. Magn. Soc. Jpn.* **24** 571–4

[16] Mitani S, Takanashi K, Yakushiji K, Chiba J and Fujimori H 2001 *Mater. Sci. Eng. B* **84** 120–5

[17] Khenata R, Daoudi B, Sahnoun M, Baltache H, Rerat M, Reshak A H, Bouhafs B, Abid H and Driz M 2005 *Eur. Phys. J. B* **47** 63-70

[18] Asano T, Ishiwara H and Kaifu N 1983 *Jan. J. Appl. Phys.* **22** 1474-81

[19] Hosoya H, Arita M, Hamada K and Takahashi Y 2006 *Mat. Sci. Eng. C* **26** 1146-50

[20] Gray Dwight E 1957 *American Institute of Physics Handbook Second Edition* New York McGraw-Hill Book Company Inc. 9-22-95

[21] Wagner C D, Riggs W M, Davis L E and Moulder J F 1979 *Handbook of X-ray Photoelectron Spectroscopy* Muikenberg G E Minnesota Parkin-Elmer Corporation Physical Electronics Division 44–97

[22] Helmolt R v, Wecker J and Samwer K 1994 *Phys. Stat. Sol. (b)* **182** K25–9

[23] Ferrari E F, da Silva F C S and Knobel M 1997 *Phys. Rev. B* **56** 6086-93

Captions

Fig. 1

(a)–(c) AFM images of granular films with 26, 52, and 63 vol.% Fe. Films were deposited at T_s = 300 K. (d) Surface roughness of films vs. Fe volume fraction. (e) STM image and (f) cross-sectional TEM image of sample with about 30 vol.% Fe.

Fig. 2

XPS spectra of film with 31 vol.% Fe for (a) Fe 2p, (b) Sr 3d, and (c) F 1s. Arrow in (a) indicates peak position of Fe $2p_{3/2}$ of FeF_2.

Fig. 3

Typical examples of (a) ρT, (b) ρ vs $1/T^{-1/2}$, (c) MH and (d) MR curves of film showing TMR (35 vol.% Fe).

Fig. 4

(a) MH curve from Fig. 3 (b) on which fitted curve using Eq. (5) is superposed. (b) Particle size distribution obtained. Analyzed statistical median d_m, geometric standard deviation σ, and average diameter d_{ave} are also indicated in graph.

Fig. 5

(a) Resistivity and (b) MR ratio summarized as functions of Fe fraction. Open and filled circles denote data measured at 300 and 77 K, respectively. Diamonds in (a) are data for Fe-MgO (T_s = 300 K) measured at 300 K.

Fig. 6

(a) Typical SEM image showing top view of Fe-SrF_2 device. (b) Current-voltage (I_d-V_d) curves of sample measured at 8 K (left scale, solid line) and at RT (right scale, dashed line). (c) Drain current I_d depending on gate voltage V_g measured at 8K. Data for three drain voltages V_d are compared.

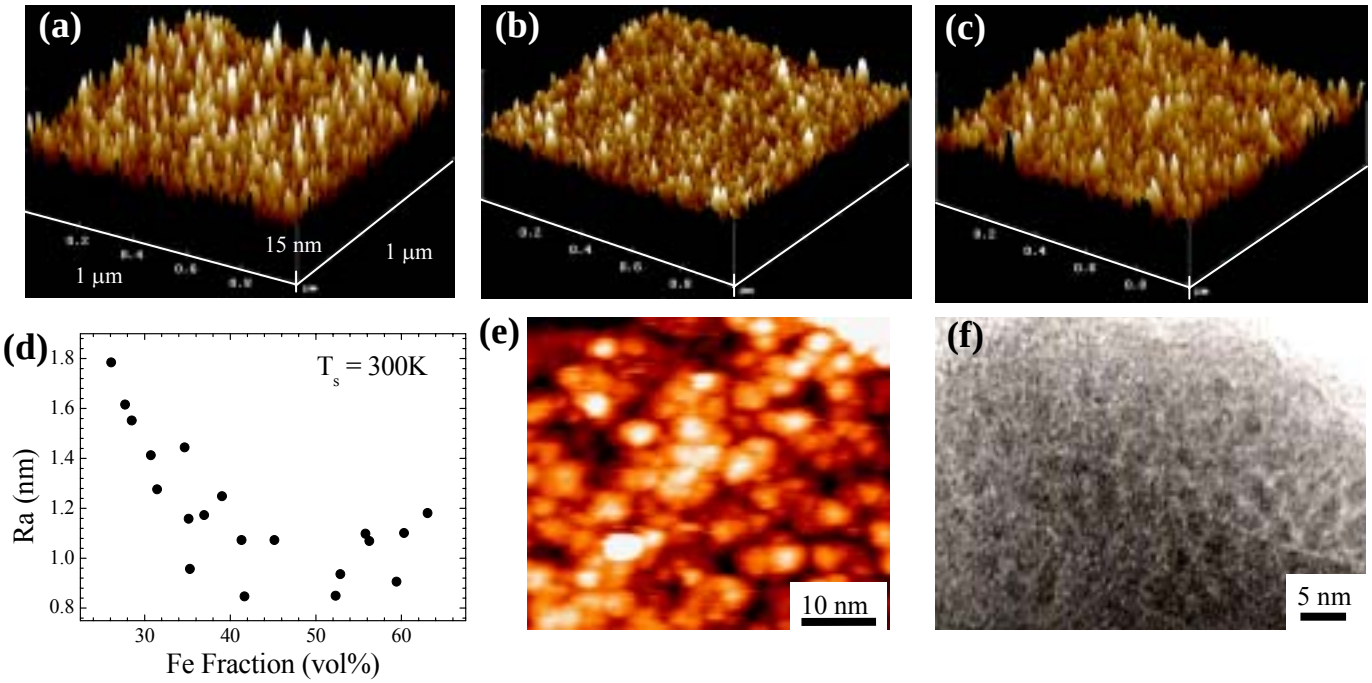


Fig. 1 H. Hosoya

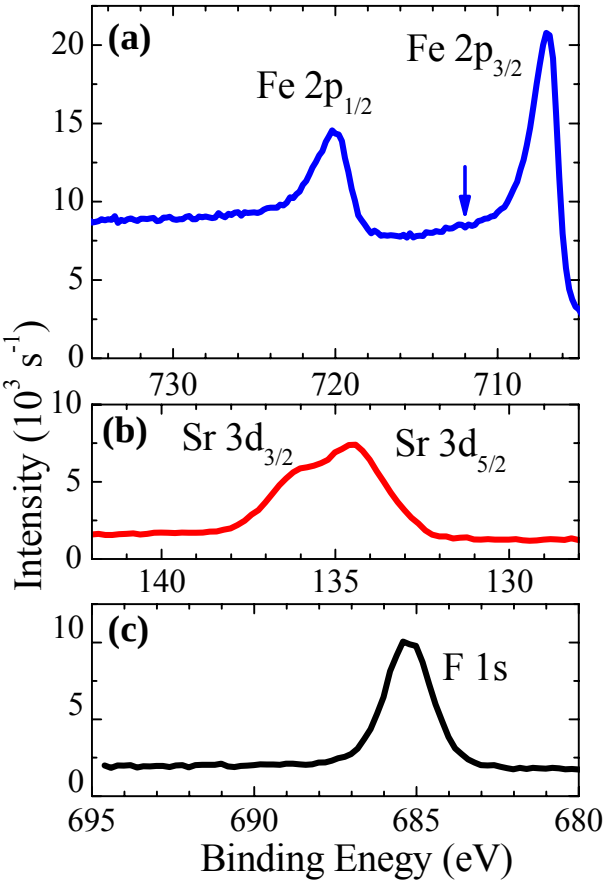


Fig. 2 H. Hosoya

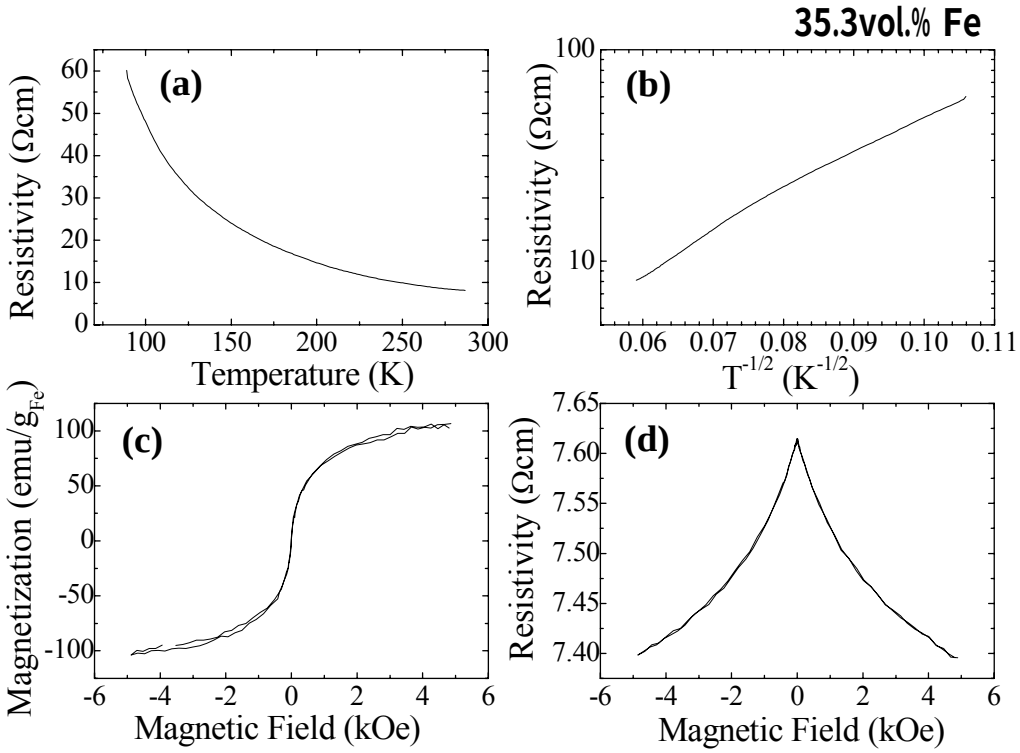


Fig. 3 H. Hosoya

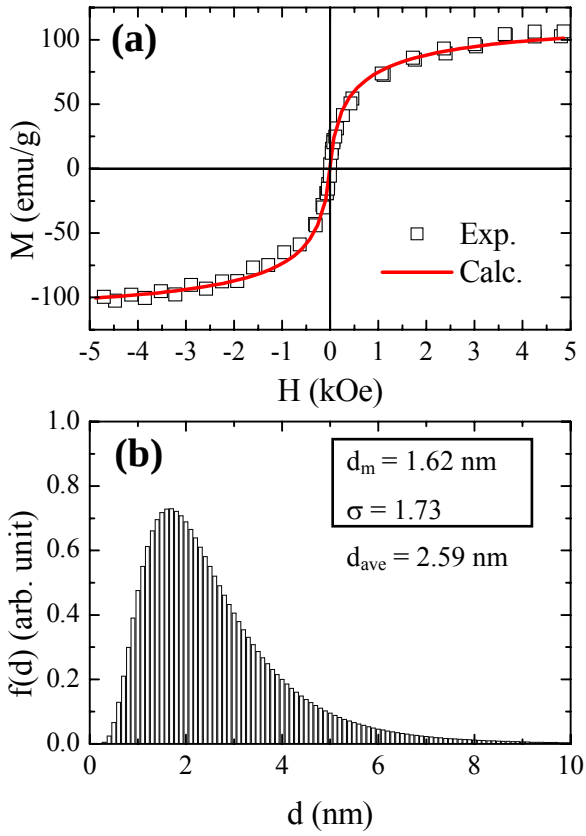


Fig. 4 H. Hosoya

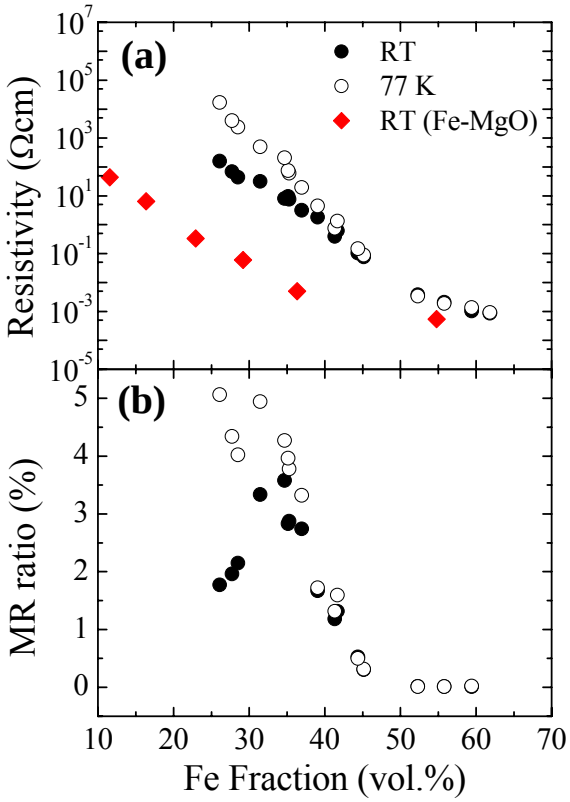


Fig. 5 H. Hosoya

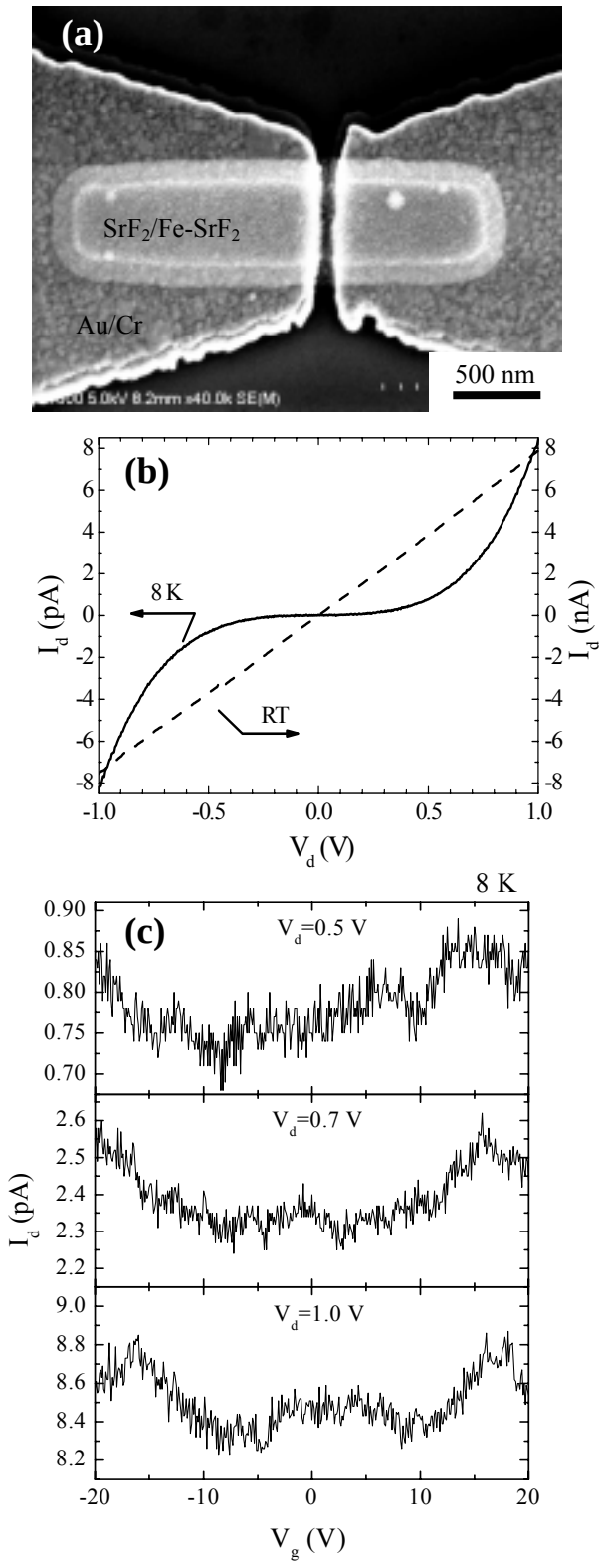


Fig. 6 H. Hosoya